



This is a repository copy of *A clinically aligned experimental approach for quantitative characterization of patient-specific cardiovascular models*.

White Rose Research Online URL for this paper:
<http://eprints.whiterose.ac.uk/160153/>

Version: Published Version

Article:

Narata, A.P., Silva de Moura, F., Patat, F. et al. (6 more authors) (2020) A clinically aligned experimental approach for quantitative characterization of patient-specific cardiovascular models. *AIP Advances*, 10 (4). 045106.

<https://doi.org/10.1063/1.5141350>

Reuse

This article is distributed under the terms of the Creative Commons Attribution (CC BY) licence. This licence allows you to distribute, remix, tweak, and build upon the work, even commercially, as long as you credit the authors for the original work. More information and the full terms of the licence here:
<https://creativecommons.org/licenses/>

Takedown

If you consider content in White Rose Research Online to be in breach of UK law, please notify us by emailing eprints@whiterose.ac.uk including the URL of the record and the reason for the withdrawal request.






eprints@whiterose.ac.uk
<https://eprints.whiterose.ac.uk/>

A clinically aligned experimental approach for quantitative characterization of patient-specific cardiovascular models

Cite as: AIP Advances **10**, 045106 (2020); <https://doi.org/10.1063/1.5141350>

Submitted: 04 December 2019 . Accepted: 15 March 2020 . Published Online: 03 April 2020

Ana Paula Narata, Fernando Silva de Moura , Frédéric Patat, Alberto Marzo, Ignacio Larrabide, Jean-Marc Gregoire , Cecile Perrault, Charles A. Sennoga, and Ayache Bouakaz 



View Online



Export Citation



CrossMark

ARTICLES YOU MAY BE INTERESTED IN

[Particle Residence Time in pulsatile post-stenotic flow](#)

Physics of Fluids **32**, 045110 (2020); <https://doi.org/10.1063/1.5144388>

[On hysteresis based random number generation](#)

AIP Advances **10**, 045308 (2020); <https://doi.org/10.1063/1.5129981>

[Acoustic wave sparsely activated localization microscopy \(AWSALM\): Super-resolution ultrasound imaging using acoustic activation and deactivation of nanodroplets](#)

Applied Physics Letters **113**, 014101 (2018); <https://doi.org/10.1063/1.5029874>

NEW!

Sign up for topic alerts
New articles delivered to your inbox



A clinically aligned experimental approach for quantitative characterization of patient-specific cardiovascular models

Cite as: AIP Advances 10, 045106 (2020); doi: 10.1063/1.5141350

Submitted: 4 December 2019 • Accepted: 15 March 2020 •

Published Online: 3 April 2020



Ana Paula Narata,^{1,a)} Fernando Silva de Moura,^{2,b)}  Frédéric Patat,^{1,a)} Alberto Marzo,³ Ignacio Larrabide,⁴ Jean-Marc Gregoire,¹  Cecile Perrault,³ Charles A. Sennoga,¹ and Ayache Bouakaz¹ 

AFFILIATIONS

¹UMR 1253, iBrain, Université de Tours, Inserm, 37032 Tours, France

²Engineering, Modeling and Applied Social Sciences Center, Universidade Federal do ABC, 09606-070 São Paulo, Brazil

³Mechanical Engineering Department, INSIGNEO Institute for in silico Medicine, University of Sheffield, S1 3JD Sheffield, United Kingdom

⁴PLADEMA-CONICET, Universidad Nacional del Centro de la Provincia de Buenos Aires, Pinto 399, CP 7000 Tandil, Argentina

^{a)}Also at: Interventional Neuroradiology, CHRU Hôpitaux de Tours, 37044 Tours, France.

^{b)}Author to whom correspondence should be addressed: fernando.moura@ufabc.edu.br

ABSTRACT

Recent improvements in computational tools opened the possibility of patient-specific modeling to aid clinicians during diagnosis, treatment, and monitoring. One example is the modeling of blood flow for surgical planning, where modeling can help predict the prognosis. Computational analysis is used to extract hemodynamic information about the case; however, these methods are sensitive to assumptions on blood properties, boundary conditions, and appropriate geometry accuracy. When available, experimental measurements can be used to validate the results and, among the modalities, ultrasound-based methods are suitable due to their relative low cost and non-invasiveness. This work proposes a procedure to create accurate patient-specific silicone replicas of blood vessels and a power Doppler compatible experimental setup able to simulate and measure realistic flow conditions. The assessment of silicone model geometry shows small discrepancies between these and the target geometries (median of surface error lies within 57 μm and 82 μm). Power Doppler measurements were compared against computational fluid dynamics results, showing discrepancies within 10% near the wall. The experimental approach offers a setup to quantify flow in *in vitro* systems and provide more accurate results where other techniques (e.g., particle image velocimetry and particle tracking velocimetry) have shown limitations due to the interference of the interface.

© 2020 Author(s). All article content, except where otherwise noted, is licensed under a Creative Commons Attribution (CC BY) license (<http://creativecommons.org/licenses/by/4.0/>). <https://doi.org/10.1063/1.5141350>

I. INTRODUCTION

Patient-specific modeling has gained new momentum over the past two decades, mainly driven by improvements in computer power, modeling software, the availability of high-resolution medical imaging techniques, and the potential of biomechanical measurements for clinical decision-making and surgical planning.¹ Of fundamental importance for a successful translation of such modeling approaches toward clinical utility is their reliability in providing robust and accurate predictions, a requisite that can be achieved

through a process of verification, validation, and assessment of the impact of data uncertainty (variable, noisy, or missing data) on the model outputs. Specifically in cardiovascular studies, many experimental approaches have been proposed by the scientific community for validation of modeled data ranging from optical-based techniques, such as Particle Image Velocimetry (PIV)^{2,3} and Particle Tracking Velocimetry (PTV), to measurements obtained using approaches that are more aligned with current clinical procedures such as ultrasound (US)/echo Doppler and MRI for quantification of blood flows *in vitro* and *in vivo*.⁴⁻⁸

Of particular interest for their relatively low costs, minimal invasiveness, and ubiquitous presence in clinical settings is the use of ultrasound-based approaches. Most studies reported in the literature using ultrasound-based techniques, however, are only capable of capturing a reduced amount of flow data often lacking spatial resolution, a limiting factor in the context of quantitative modeled-data validation. In an attempt to provide a more quantitative and accurate approach for the analysis of flow in 2D images, de Senneville *et al.*⁹ proposed a combination of contrast-enhanced ultrasound (CEUS) with modeling to enhance measurement accuracy. This led to improved accuracy of the measured data compared to more traditional ultrasound-based approaches, paving the way to the establishment of such techniques for quantitative analysis of blood flows. The aim of this study is to develop closely matching experimental patient-specific 3D anatomical replicas and evaluate ultrasound power Doppler (PD) flow measurements as a way to characterize the flow in these replicas. Geometry quality assessment is performed to quantify the quality of the models, and PD measurements are compared against the Computational Fluid Dynamics (CFD) analysis to quantify the discrepancy between the results.

The approach will be tested in the clinical context of analyzing blood flow through arterial bifurcations affected by an intracranial aneurysm (IA).

II. METHODS

A. Patient data selection and 3D geometry segmentation

To produce true-to-scale patient-specific replicas of bifurcations, we used 3DRA images from our retrospectively maintained database of patients presenting to clinic with unruptured IAs. Informed consent was obtained from all participants, and institutional ethical approval was in place for research use of patient radiological data. The study was approved by the local institutional review board (Comité de Protection des Personnes de Tours, France) in accordance with French legislation and European Union guidelines. The @neurIST computational tool chain was used for segmentation and extraction of the surface mesh from 3DRA images, following the literature.^{10,11} The software Blender[®] was also employed for further mesh manipulation. To reduce vascular complexity in patient-specific replicas, wherever appropriate, small tertiary-branches were eliminated from the models due to their negligible effect on local hemodynamics. In total, six patients with intracranial aneurysm were selected (1 ACOM, 4 MCA, and 1 ACA).

Segments of the idealized bifurcating vasculature were also generated *in silico*, for further testing. Blood flow is a complex phenomenon, highly dependent on boundary conditions and the geometry of the vessel. The simplified geometry of the idealized bifurcations allows for better control of the ultrasound experimental setup and thus can be used as a benchmark test for ultrasound measurement techniques. The geometries of two idealized cases were constructed, one symmetric and one asymmetric, using the open-source software FreeCAD.¹² In both cases, the afferent vessel diameter was set to represent an average size of the vessels located near the Circle of Willis. Branching vessels were defined in accordance with Murray's law.¹³

B. Silicone model construction

Replicas of patient-specific bifurcation aneurysm and idealized geometries were produced from the segmented vessel surfaces. At each inlet and outlet, a diameter transition segment was added for easy connection with the circulatory loop. The transition was designed with a small angle to avoid singular head losses.¹⁴

The physical molds representing the patient or idealized vascular bifurcations were generated by means of rapid prototyping by using a Stratasys Objet30 3D printer (Stratasys Solutions[®] Limited, Cambridge, United Kingdom) with an acrylic compound (VeroWhitePlus RGD835, Stratasys Solutions). The positive models were carefully polished to remove any artifact left by the 3D printer. Figure 1(a) shows the positive mold after polishing. The positive molds were printed hollow with a wall thickness of 1.5 mm for easier mold removal in the subsequent stages of construction.

A housing case was employed to enclose the silicone during the curing process. The housing was designed by offsetting the positive mold outward by 2 mm, providing space between the housing and the positive mold for silicone composite injection. The offset was chosen to ensure mechanical robustness of the replica while at the same time minimizing excessive attenuation during ultrasound investigations. The housing was designed in two parts, allowing easy extraction after the curing process. Holes were drilled in the housing to allow the silicone composite to be injected into the space between the positive mold and the housing. Figure 1(b) shows the parts that compose the housing for one of the cases with the three-way taps attached. The number and locations must be chosen, case by case, to minimize chances of trapping air during the silicone injection procedure. A three-way tap was glued in each hole to connect the syringes with the silicone composite.

Figure 1(c) shows the positive mold inside the housing. The only points of contact between the positive mold and the housing are at the ends of the inlet and outlets of the replicas. A thin layer of

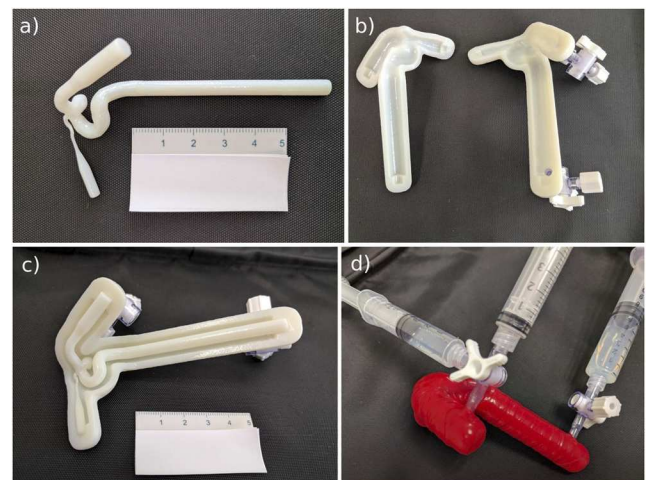


FIG. 1. Silicone model construction. (a) 3D printed positive mold after polishing. (b) Housing parts. One of the parts was drilled and glued to three-way taps used to inject the silicone compound. (c) Positive mold inside the housing. (d) Positive mold and housing sealed with an elastic rubber band and ready for silicone injection.

silicone oil was applied to the interior part of the housing to facilitate later model extraction. Silicone oil must not be applied to the positive mold to avoid surface artifacts. The housing was carefully closed around the positive mold and sealed with an elastic rubber band for silicone injection through the three-way taps. No glue was used so that the housing could be reused. Figure 1(d) presents the set ready for silicone composite injection.

The material used to construct the replicas was a robust, curable, and transparent silicone composite of XIAMETER® RTV-4234-T4 base and curing agent (SAMARO, Thouare sur Loire, France). After mixing the composite, the entire volume was introduced in a vacuum chamber to remove air bubbles before injection to minimize undesired ultrasound wave scattering during the experiments. Silicone was slowly injected while orienting the housing such that the silicone filled the interior gap from the bottom. Prior to the injection, the model must be oriented in space to avoid the formation of air traps while the silicone level rises from the bottom.

After curation, the housing was carefully opened to extract the silicone model, together with the positive mold inside. The silicone model with the positive mold was then immersed in dichloromethane to remove the printed material within while keeping the silicone model intact. The printed material becomes fragile and brittle in contact with dichloromethane and can be carefully carved from inside the model using a thin wire inserted along its openings. Care must be taken during this process since the silicone becomes fragile while soaked in the solvent. After the removal, the silicone replica was left to rest for 24 h at room temperature, allowing for dichloromethane evaporation. The silicone models showed no structural integrity damages after the solvent evaporated.

C. Model geometry assessment

The geometry accuracy of patient-specific replicas was quantitatively assessed. Each replica's vessel surface was compared against its target, i.e., the surface used to print the model (and also to run the CFD analysis). First, each replica was filled with an x-ray contrast agent (Iopamiron 300, Guerbet, France), and 3DRA images were acquired. The 3D surfaces of the replicas were then extracted using the same procedure described before and were aligned with their target surfaces using a mesh registration algorithm [Iterative Closest Point (ICP) alignment method], implemented as a Blender custom plugin.¹⁵

After the alignment, the error between each model and its target was computed as follows.¹⁶ For each vertex pertaining to the replica's 3D surface S_R , the spatial position error index with respect to the target surface S_T is given by

$$\text{error}(\vec{P}_R, S_T) = \min_{\vec{P}_T \in S_T} \|\vec{P}_R - \vec{P}_T\|_2, \quad (1)$$

where \vec{P}_R and \vec{P}_T are the coordinates of points pertaining to S_R and S_T , respectively, and $\|\cdot\|_2$ is the Euclidean distance operator. This error index is computed for each vertex of S_R and projected over the surface for visualization.

D. Ultrasound experimental setup

The experimental setup used for ultrasound flow measurements is presented in Fig. 2. An ultrasound system (Aixplorer®

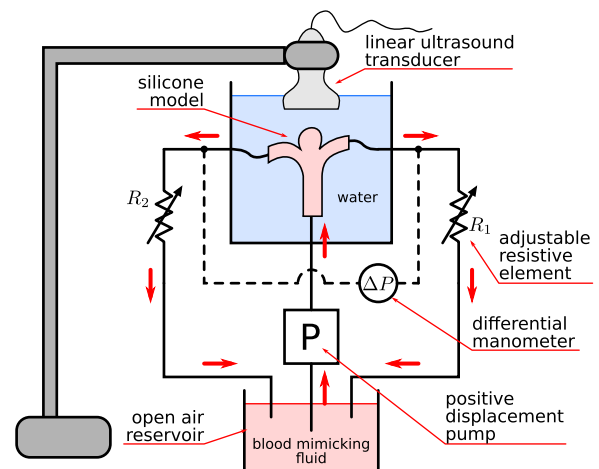


FIG. 2. Ultrasound-compatible circulatory loop showing the arrangement of the resistive elements, 3D bifurcation replica, positive displacement pump, and ultrasound transducer.

Multiwave SuperSonic Imagine, S.A.; Aix-en-Provence, France) equipped with a 256-element (SL15-4) 7.5 MHz linear-array transducer was used to capture real time ultrasound images. The transducer was fixed to a rigid mechanical holder with a 3D rotational and metered translation stage. An ultrasound-compatible mock circulatory loop was connected to a CompuFlow 1000 positive displacement pump (Shelley Medical Imaging Technologies, Toronto, Canada) capable of generating realistic cerebral blood flow. The model replicas were immersed in a water tank ($30 \times 30 \text{ cm}^2$) to allow coupling between the transducer and the replicas.

Ultrasound-compatible blood mimicking fluid (Model 046 CRS, Tissue Simulation Technology, VA, USA) with nominal density $\rho = 1050 \text{ kg/m}^3$ at an ambient temperature of $22 \text{ }^\circ\text{C}$ and nominal dynamic viscosity $\mu = 4.0(5) \text{ mPa}\cdot\text{s}$ approximating that of blood was used as the working fluid. A magnetic stirrer incorporated into the reservoir ensured uniform distribution of the ultrasound scattering particles within the blood mimicking fluid. Timed collection and volume measurements of the blood mimicking fluid in a volumetric flask (flow rates ranging from 0.1 ml/s to 10 ml/s) were performed to calibrate the flow meter and to measure the flow output of the pump.

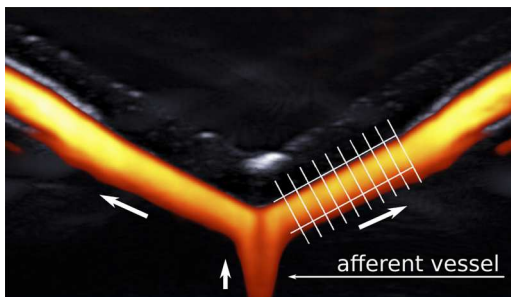
Tubing to-and-from the pump was used to connect the silicone replicas into the circulation loop. The connecting tubing diameters were considerably larger than the distal vessel diameters to minimize additional hydraulic head loss that may adversely alter the desired distribution of flow and hydraulic resistances at the interface with the phantoms. A differential manometer was connected to the distal part of the tubing, close and equally distant from the outlets. The distal part of the tubing was disposed horizontally to avoid hydrostatic pressure differences between the branches. Adjustable resistive elements (metered taps) were used to set the desired peripheral resistances.

E. Computational fluid dynamics analyses

In order to validate the fluid dynamics inside the replicas, it would be necessary to accurately measure velocity profiles in small

TABLE I. Boundary conditions imposed for each CFD analysis.

Case	Inlet flow rate (ml/s)	Terminal resistance (mmHg · s/ml)
Idealized (symmetric)	0.976	55
Idealized (asymmetric)	0.976	55
Patient 1 (ACOM)	1.25	80
Patient 2 (MCA)	2.30	75
Patient 3 (MCA)	2.30	75
Patient 4 (MCA)	2.30	75
Patient 5 (ACA)	1.25	80
Patient 6 (MCA)	2.30	75

**FIG. 3.** Time-averaged PD flow image, superposed with the B-mode of the symmetric idealized geometry near the bifurcation. White arrows indicate flow directions, and the two long parallel lines mark the fluid/wall interface of one of the branching vessels. The multiple short parallel lines represent the cross-sectional lines where velocity profiles were extracted.

arteries of the brain of patients. Since this type of measurement is not currently feasible due to difficulties in accessing the arteries, this study focused on quantifying discrepancies between PD measurements and a CFD model. The 3D Navier–Stokes equations were solved by using the finite-control-volume software, ANSYS® CFX. Steady state flow analysis was performed,¹⁷ assuming Newtonian incompressible blood with density $\rho = 1050 \text{ kg/m}^3$ and viscosity $\mu = 3.5 \text{ mPa} \cdot \text{s}$. Tetrahedral elements were used to discretize the

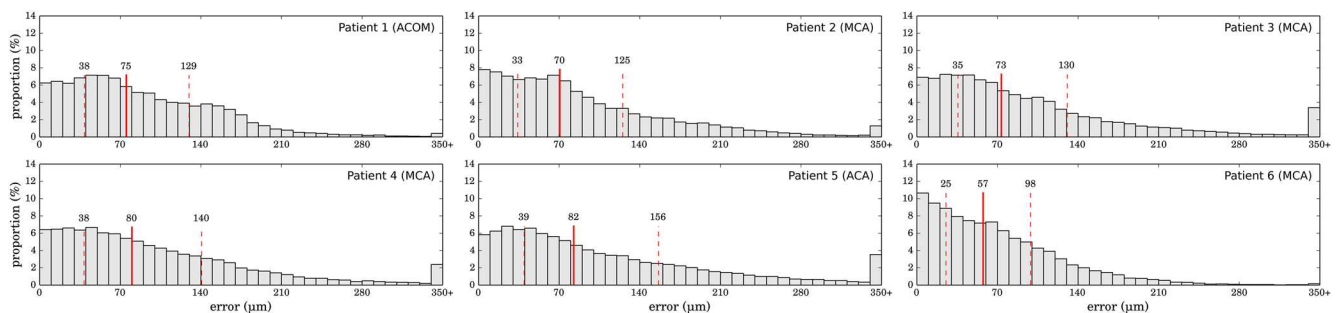
core of the computational domain, with three layers of prismatic elements at the wall to ensure accurate computation of velocity gradients. Grid sizes with an average density of at least 2400 el/mm^3 were used following the recommended discretization approach for stented geometries.^{18–21} Fully developed parabolic velocity profiles were imposed at all inlet boundaries, resulting in typical volumetric flow rate values at those anatomical locations. Outlet boundaries were defined as peripheral resistances rather than pressure or velocity values that might unintentionally alter peripheral resistances down the bifurcating vessels.^{22,23} Table I shows the boundary conditions imposed for each CFD analysis. Flow rates are representative of average flow rates in these vessels. Peak systolic and diastolic flow rates were also evaluated; however, no significant differences were observed.

Numerical analyses were run in parallel using 2 Intel Ivy Bridge based HPC cluster nodes (each node uses 2 Intel E5 2650V2 8-core processors, 4 GB RAM). The average time required to solve an analysis was 20 h.

F. Ultrasound flow measurement and image post-processing

After verifying the absence of leaks and complete exclusion of trapped air bubbles within the circulatory loop, the inlet flow rate was adjusted to match those used in the CFD analyses. Peripheral resistances were adjusted in each case by comparing the differential pressure measured with the manometer attached to the circulatory loop and the difference in the static pressure between the outlets obtained from the CFD analysis while maintaining the same flow rates.

Measurements were conducted at steady flow rates. The flow within the replicas was assessed using power Doppler ultrasound imaging, using a pulse repetition frequency of 1.95 kHz. The PD velocity scale was adjusted for each case, maximizing the resolution near the wall where velocities are smaller. The focus is to evaluate the flow near the interface where measurement is more challenging and other velocity measurement techniques present limitations. As a consequence, it is expected that saturation and artifacts appear deeper into the flow where velocities are higher.²⁴ For each replica, the ultrasonography PD protocol consisted of 15 s acquisitions and one frame in B-mode at the same position. For all idealized planar replicas, PD flow images were acquired in the

**FIG. 4.** Histograms of the position error for all patient-specific geometries. The red continuous lines indicate the median, and the red dashed lines represent quartiles Q1 and Q3.

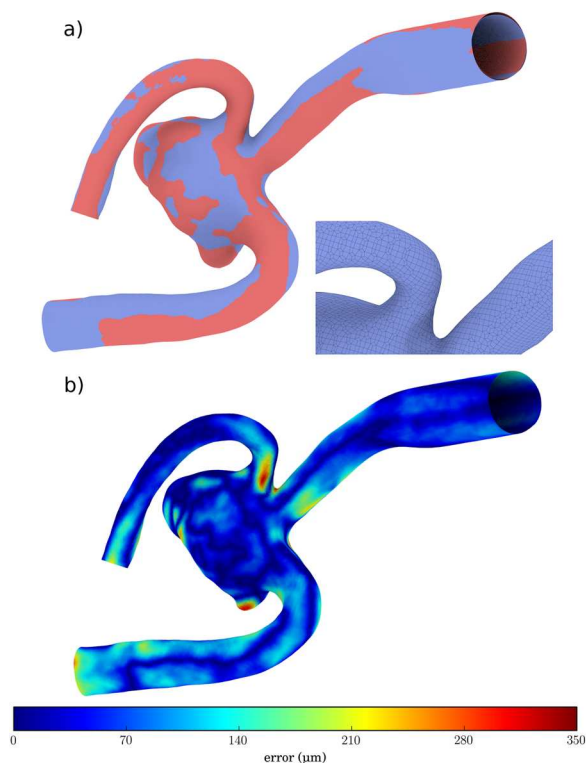


FIG. 5. Bifurcation surface mesh assessment of patient 6. (a) Silicone model surface mesh (blue) and target mesh (red) superposed after mesh registration. The zoomed-in picture presents the distribution of surface mesh vertices of both surfaces. (b) Computed error index mapped in the surface of the replica.

bifurcation plane across the entire replica. In contrast, PD flow images for patient-specific replicas were acquired every 1 mm across the model, controlled by the mechanical holder with metered translation. The resultant data were transferred to a personal computer for further analysis.

A post-processing analysis sequence was performed. For each idealized case, the sequence comprised the following steps: (i) compute a time-averaged PD image from the 15 s acquisition, (ii) use B-mode image to locate the walls of the vessels and adjust the spatial scale of the images, (iii) velocity profile extraction along the distal vessels from the time-averaged PD image, and (iv) extraction of velocity profiles from the CFD results at the same locations. Figure 3 shows the time-averaged image used to extract velocity profiles for one of the idealized geometry datasets.

In the case of patient-specific replicas, the steps were as follows: (i) for each plane of measurement, compute a time-averaged PD image from the 15 s acquisition; (ii) build a 3D map of velocities within the blood vessel using PD measurements and plane locations; (iii) extract the geometry of the vessel from B-mode images or the PD velocity isosurface near the wall and align it with the surface of the vessel used in the CFD analysis; (iv) find a base transformation matrix between the reference system used in CFD and PD measurements; (v) locate the PD measurement planes in the CFD reference system and extract CFD velocity values; and (vi) extract velocity profiles from PD measurements and CFD results at the same locations in these planes.

III. RESULTS

In total, six silicone models of different patients were produced in addition to two other models with idealized geometries. For each patient case, geometry accuracy was quantitatively assessed

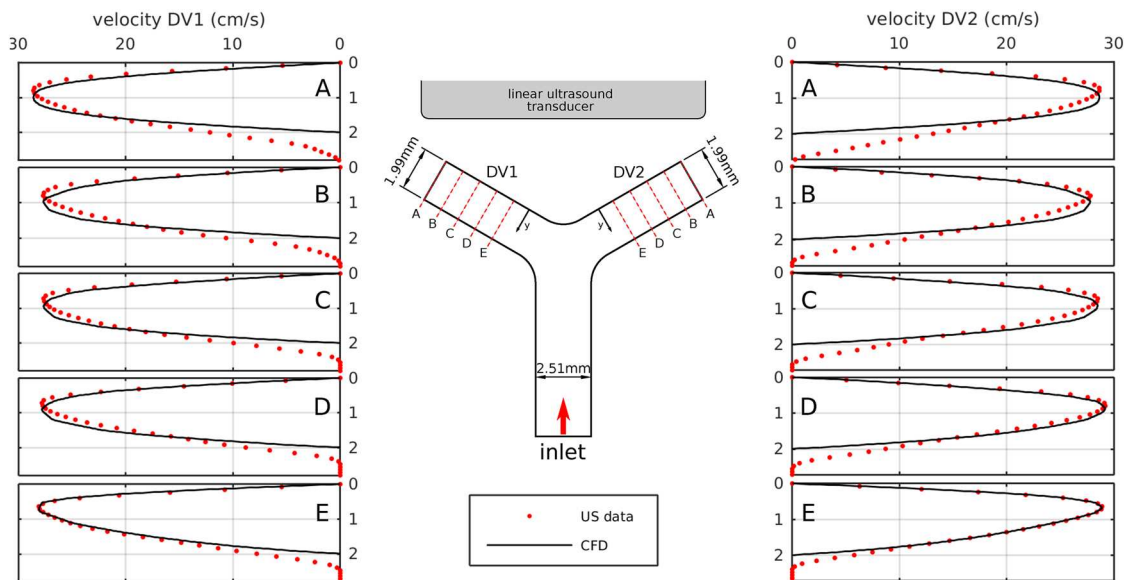


FIG. 6. Velocity profile comparison of the idealized symmetric bifurcation model. The graphs present the profiles obtained from the CFD analysis (black continuous line) and ultrasound PD measurements (red dots). The location of each profile is indicated in the central diagram.

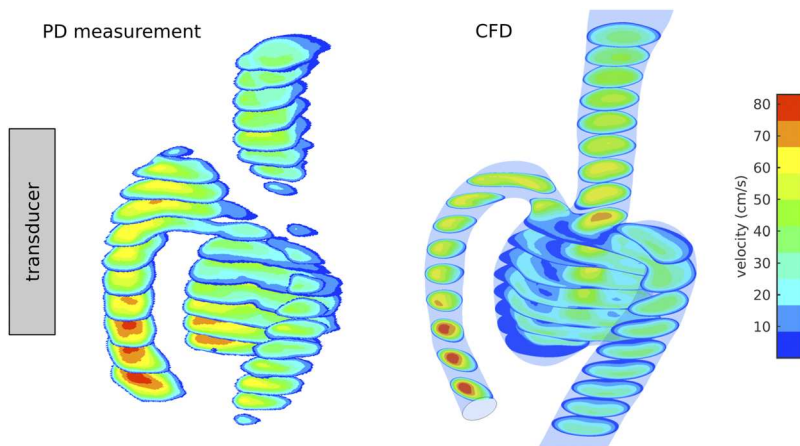


FIG. 7. Velocity contour plots of patient 6. Power Doppler measurements (left) and CFD analysis (right).

using the error index. CFD analysis was performed, and PD data were acquired following the experimental procedure described earlier for each idealized geometry and two representative patient cases, one MCA and one ACA, since these are common locations for intracranial aneurysms.

The analysis of the results is divided in two: First, the accuracy of the models was assessed by comparing the vessels of the patients extracted from 3DRA images and the surfaces of the produced replicas. Second, ultrasound PD measurements were compared to CFD results.

A. Geometry assessment of patient replicas

All replica surfaces were aligned with their targets, and the surface error index (1) was computed. Figure 4 presents histograms of

the error index for all patients. The medians lie within $57 \mu\text{m}$ and $82 \mu\text{m}$. Figure 5(a) depicts a representative example of the meshes superimposed after mesh registration. Figure 5(b) show the error index mapped into the surface of the replica in μm . While there are a few locations with larger error ($>280 \mu\text{m}$), most of the surface has much smaller error ($<70 \mu\text{m}$).

B. Fluid dynamic assessment

Velocity profiles extracted from CFD and PD measurements of one of the symmetric idealized cases are presented in Fig. 6. The transducer location is also identified in the central diagram. The results show close quantitative alignment between the measured and modeled data on the side of the vessel (up to 1.2 mm) near the position of the ultrasound transducer and progressively worse alignment

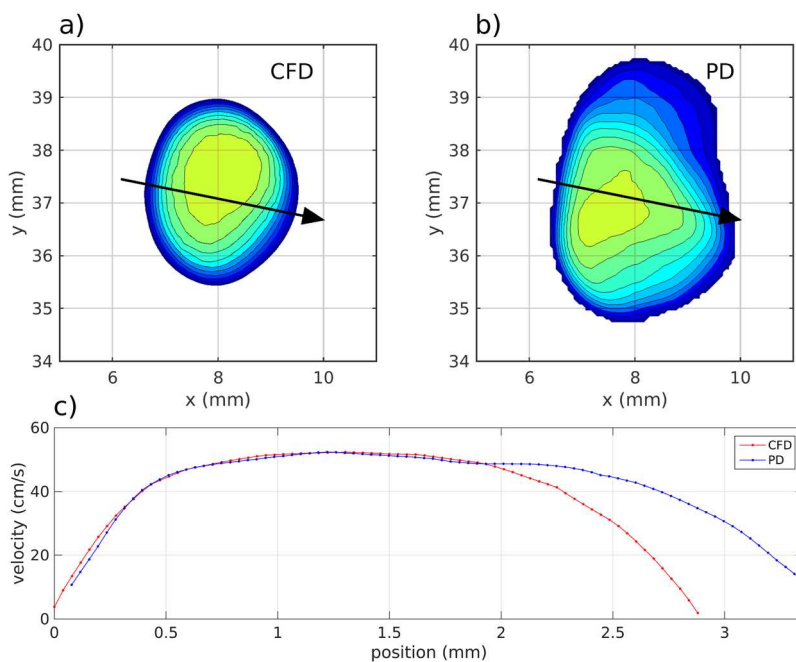


FIG. 8. Velocity profile comparison of the patient-specific cases. (a) CFD results. (b) Power Doppler measurements. (c) Velocity profiles comparison along indicated arrows.

moving away from the transducer. As mentioned before, the focus in this study is to evaluate flow near the wall closer to the transducer; therefore, the gain was adjusted accordingly to emphasize measurements in this region in detriment to measurements deeper into the lumen of the vessel.

The velocity contour plots from PD measurements and CFD simulations of patient 6 are presented in Fig. 7. Figure 7 also shows the transducer's location during measurements.

Figure 8 shows a representative comparison between the PD measurements and the CFD simulation obtained in one location of patient 6 in the top, whereas velocity profiles along the indicated arrows in the bottom. The transducer is positioned to the left in the image. These results show similar trends to those already identified in the idealized comparison, where the results show good

alignment on the side of the vessel near the position of the ultrasound transducer.

Power Doppler velocity profiles were extracted from different positions and planes and compared against the correspondent CFD profiles. Figure 9 presents the normalized velocity difference Δv as a function of the position in the lumen of the vessel for two of the analyzed cases. The normalized velocity difference Δv is given by

$$\Delta v(x) = \frac{|v_{CFD}(x) - v_{PD}(x)|}{\max(v_{CFD}(x))} (\times 100\%), \quad (2)$$

where $\max(v_{CFD})$ is the maximum velocity of each velocity profile.

IV. DISCUSSION

The aim of this study was to develop patient-specific 3D anatomical models and to evaluate an ultrasound-based experimental approach for quantification of blood-mimicking 3D fluid flow. This work presented a method to produce true-to-scale 3D vascular replicas of cerebral vessels based on 3DRA images from patients and using 3D printing machines for quick prototyping of complex anatomical shapes that would be difficult to produce otherwise.

Replicas from six patient-specific and two idealized geometries were constructed following this procedure. The difference between the surfaces of the produced replicas and their target surfaces was evaluated quantitatively using a position error index. The median of the position error lies within $57 \mu\text{m}$ and $82 \mu\text{m}$. This would represent an average error of 5% with respect to the mean vessel nominal diameter.

A quantitative characterization of flow was performed, comparing PD measurements against CFD modeled data. The replicas were evaluated under realistic flow rates and boundary conditions using the proposed experimental setup. Flow rates and terminal resistances can be adjusted, allowing the simulation of different physiological conditions. In this work, steady state flow was used to compare ultrasound PD measurements against CFD simulations. Although transient flow has not been assessed at this time, this technique operates at a very high frequency, which enables measuring flow at a transient regime.

Ultrasound PD was used to measure velocities inside the replicas. Power Doppler ultrasound is a very sensitive technique for detection of flow and that provides reliable estimates of velocity profiles particularly in small vessels with low velocity flow at the expense of the direction information. PD velocity measurements show good agreement with CFD results near the wall closest to the transducer. The discrepancy between PD measurements and CFD analysis lies within 10% near the proximal wall up to 1.2 mm deep into the lumen of the vessels.

The same comparison degrades substantially at positions further away from the wall due to velocity gain adjustment needed to emphasize flow near the wall. High PD gains can introduce artifacts in the regions of the image far from the transducer, mainly displaying flow where flow is not present, appearing that there is flow outside the vessel in the opposite side of the transducer.²⁴ This effect can be seen in the measurements, e.g., Figs. 6 and 8.

This is a rather small price to pay for a valuable in-vivo measure such as velocity magnitude near the wall. Until today, it was not possible to assess flow in such a detailed manner, allowing to

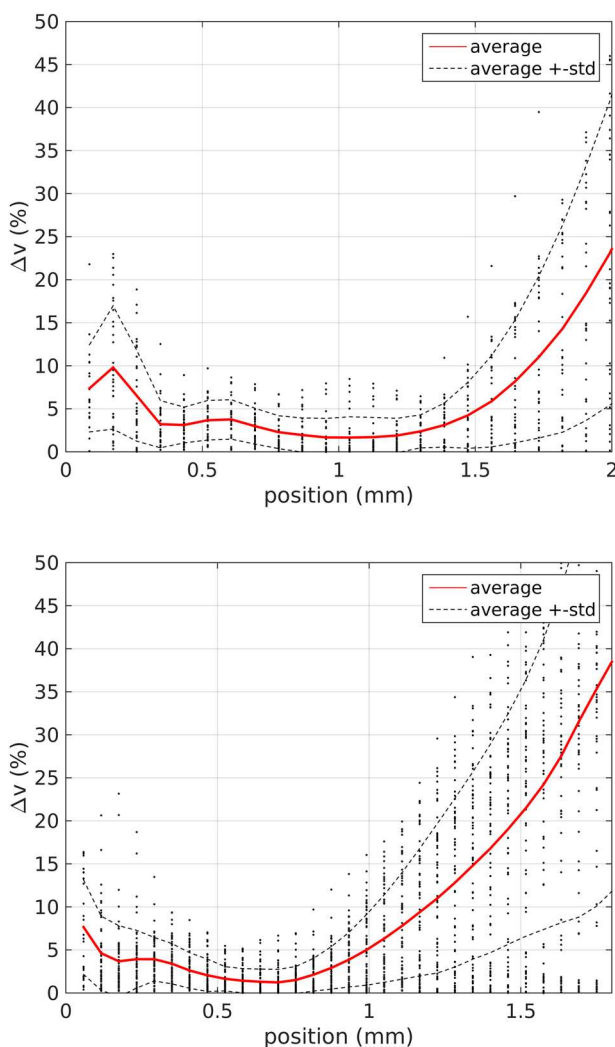


FIG. 9. Normalized velocity differences Δv of patients 5 (top) and 6 (bottom). The red continuous lines represent the average, and black dashed lines represent the average plus or minus one standard deviation. The black dots represent single difference measurements $\Delta v(x)$ from different locations across the replicas.

make measurements in patients to assess flow while comparing different conditions (before and after treatment, for instance). Recent advances in Doppler techniques such as ultrafast Doppler and super resolution Doppler should be able to improve significantly the sensitivity of this technique, reducing the need to increase gains.^{25,26}

This limitation can be overcome by reorienting the transducer with respect to the replica when measurements are required along the entire circumference of the vessel. Nevertheless, for the purpose of characterization, experimental measurements show that the flow inside the replicas match the CFD analysis.

Another limitation of this study is the absence of elastic walls. Rigid walls were considered in CFD, and the silicone models, despite the elastic nature of silicone compounds, were not produced with elasticity comparable with the real cerebral vasculature. In fact, the thickness of the walls of the replicas together with the steady state regime of the pump cancels any elastic behavior of the models, allowing a direct comparison between the measurements and a rigid wall CFD model.

Producing patient-specific replicas with realistic elastic properties is very challenging and requires intense research to use it in clinical practice. There is a major bulk of literature considering rigid walls since it is nowadays very difficult to the measure elasticity of brain vessels and to produce realistic/accurate elastic replicas. In addition, wall elasticity has a minor role in flow when compared to velocities.

At its current state, this experimental approach offers a setup to quantify flow in *in vitro* systems where the probe can be positioned near the fluid/solid interface and provide more accurate results where other techniques (e.g., PIV and PTV) have shown limitations due to the interference of the interface. In the long-term, the same ultrasound technique could be further developed to allow *in vivo* measurements for direct patient-specific blood flow measurements that better align with current clinical protocols.

AUTHOR'S CONTRIBUTIONS

C.A.S. and A.B. contributed equally to this work.

ACKNOWLEDGMENTS

We gratefully acknowledge funding from the Newton Fund Programmes of the Royal Academy of Engineering (Grant No. NRCP1415/2/20) and the funding from PICT Start-up 2015-0006, PICT 2016-0116, financed by FONCYT—ANPCYT of Argentina. We also acknowledge Stryker for the financial support and Jean-Yves Tartu during the production of the replicas.

The datasets generated during and/or analyzed during this study are available in the University of Sheffield Research Data Catalogue and Repository ORDA (Online Research Data), DOI: [10.15131/shef.data.9758636](https://doi.org/10.15131/shef.data.9758636).

REFERENCES

- ¹P. R. Hoskins, P. V. Lawford, and B. J. Doyle, *Cardiovascular Biomechanics* (Springer, 2017).
- ²M. D. Ford, H. N. Nikolov, J. S. Milner, S. P. Lownie, E. M. DeMont, W. Kalata, F. Loth, D. W. Holdsworth, and D. A. Steinman, "PIV-measured versus CFD-predicted flow dynamics in anatomically realistic cerebral aneurysm models," *J. Biomech. Eng.* **130**, 021015 (2008).
- ³M. Raschi, F. Mut, G. Byrne, C. M. Putman, S. Tateshima, F. Viñuela, T. Tanoue, K. Tanishita, and J. R. Cebral, "CFD and PIV analysis of hemodynamics in a growing intracranial aneurysm," *Int. J. Numer. Methods Biomed. Eng.* **28**, 214–228 (2011).
- ⁴S. E. Maier, D. Meier, P. Boesiger, U. T. Moser, and A. Vieli, "Human abdominal aorta: Comparative measurements of blood flow with MR imaging and multigated Doppler US," *Radiology* **171**, 487–492 (1989).
- ⁵J. M. Rubin, R. S. Adler, J. B. Fowlkes, S. Spratt, J. E. Pallister, J. F. Chen, and P. L. Carson, "Fractional moving blood volume: Estimation with power Doppler US," *Radiology* **197**, 183–190 (1995).
- ⁶G. A. Taylor, B. L. Short, L. K. Walker, and R. J. Traystman, "Intracranial blood flow: Quantification with duplex Doppler and color Doppler flow US," *Radiology* **176**, 231–236 (1990).
- ⁷E. F. Donnelly, L. Geng, W. E. Wojcicki, A. C. Fleischer, and D. E. Hallahan, "Quantified power Doppler US of tumor blood flow correlates with microscopic quantification of tumor blood vessels," *Radiology* **219**, 166–170 (2001).
- ⁸N. B. Hansen, B. S. Stonestreet, T. S. Rosenkrantz, and W. Oh, "Validity of Doppler measurements of anterior cerebral artery blood flow velocity: Correlation with brain blood flow in piglets," *Pediatrics* **72**, 526–531 (1983), <https://pediatrics.aappublications.org/content/72/4/526.full.pdf>.
- ⁹B. D. de Senneville, A. Novell, C. Arthuis, V. Mendes, P.-A. Dujardin, F. Patat, A. Bouakaz, J.-M. Escoffre, and F. Perrotin, "Development of a fluid dynamic model for quantitative contrast-enhanced ultrasound imaging," *IEEE Trans. Med. Imaging* **37**, 372–383 (2018).
- ¹⁰A. Marzo, P. Singh, P. Reymond, N. Stergiopoulos, U. Patel, and R. Hose, "Influence of inlet boundary conditions on the local haemodynamics of intracranial aneurysms," *Comput. Methods Biomech. Biomed. Eng.* **12**, 431–444 (2009).
- ¹¹M. C. Villa-Uriol, G. Berti, D. R. Hose, A. Marzo, A. Chiarini, J. Penrose, J. Pozo, J. G. Schmidt, P. Singh, R. Lycett, I. Larrabide, and A. F. Frangi, "@neurIST complex information processing toolchain for the integrated management of cerebral aneurysms," *Interface Focus* **1**, 308–319 (2011).
- ¹²See www.freecadweb.org for FreeCAD; accessed 11 June 2019.
- ¹³Y. C. Fung, "Blood flow in arteries," in *Biomechanics: Circulation* (Springer New York, 1997), pp. 118–125.
- ¹⁴P. J. Pritchard, *Fox and McDonald's Introduction to Fluid Mechanics* (Wiley, 2011).
- ¹⁵A. Curtis, "Icp alignment addon for blender," https://github.com/patmo141/object_alignment; accessed 30 April 2019.
- ¹⁶P. Cignoni, C. Rocchini, and R. Scopigno, "Metro: Measuring error on simplified surfaces," *Comput. Graphics Forum* **17**, 167–174 (1998).
- ¹⁷A. J. Geers, I. Larrabide, H. G. Morales, and A. F. Frangi, "Approximating hemodynamics of cerebral aneurysms with steady flow simulations," *J. Biomech.* **47**, 178–185 (2014).
- ¹⁸A. G. Radaelli, L. Augsburger, J. R. Cebral, M. Ohta, D. A. Rüfenacht, R. Balossino, G. Benndorf, D. R. Hose, A. Marzo, R. Metcalfe, P. Mortier, F. Mut, P. Reymond, L. Succi, B. Verheghe, and A. F. Frangi, "Reproducibility of haemodynamical simulations in a subject-specific stented aneurysm model—A report on the virtual intracranial stenting challenge 2007," *J. Biomech.* **41**, 2069–2081 (2008).
- ¹⁹D. A. Steinman, Y. Hoi, P. Fahy, L. Morris, M. T. Walsh, N. Aristokleous, A. S. Anayiotos, Y. Papaharilaou, A. Arzani, S. C. Shadden, P. Berg, G. Janiga, J. Bols, P. Segers, N. W. Bressloff, M. Cibis, F. H. Gijzen, S. Cito, J. Pallarés, L. D. Browne, J. A. Costelloe, A. G. Lynch, J. Degroote, J. Vierendeels, W. Fu, A. Qiao, S. Hodis, D. F. Kallmes, H. Kalsi, Q. Long, V. O. Kheyfets, E. A. Finol, K. Kono, A. M. Malek, A. Lauric, P. G. Menon, K. Pekkan, M. E. Moghadam, A. L. Marsden, M. Oshima, K. Katagiri, V. Peiffer, Y. Mohamied, S. J. Sherwin, J. Schaller, L. Goubergrits, G. Usera, M. Mendina, K. Valen-Sendstad, D. F. Habets, J. Xiang, H. Meng, Y. Yu, G. E. Karniadakis, N. Shaffer, and F. Loth, "Variability of computational fluid dynamics solutions for pressure and flow in a giant aneurysm: The ASME 2012 summer bioengineering conference CFD challenge," *J. Biomech. Eng.* **135**, 021016 (2013).

- ²⁰K. Valen-Sendstad, A. W. Bergersen, Y. Shimogonya, L. Goubergrits, J. Bruening, J. Pallares, S. Cito, S. Piskin, K. Pekkan, A. J. Geers, I. Larrabide, S. Rapaka, V. Mihalef, W. Fu, A. Qiao, K. Jain, S. Roller, K.-A. Mardal, R. Kamakoti, T. Spirka, N. Ashton, A. Revell, N. Aristokleous, J. G. Houston, M. Tsuji, F. Ishida, P. G. Menon, L. D. Browne, S. Broderick, M. Shojima, S. Koizumi, M. Barbour, A. Aliseda, H. G. Morales, T. Lefèvre, S. Hodis, Y. M. Al-Smadi, J. S. Tran, A. L. Marsden, S. Vaippummadhom, G. A. Einstein, A. G. Brown, K. Debus, K. Niizuma, S. Rashad, S.-i. Sugiyama, M. O. Khan, A. R. Updegrove, S. C. Shadden, B. M. W. Cornelissen, C. B. L. M. Majoie, P. Berg, S. Saalfeld, K. Kono, and D. A. Steinman, “Real-world variability in the prediction of intracranial aneurysm wall shear stress: The 2015 international aneurysm CFD challenge,” *Cardiovasc. Eng. Technol.* **9**, 544–564 (2018).
- ²¹M. O. Khan, K. Valen-Sendstad, and D. A. Steinman, “Narrowing the expertise gap for predicting intracranial aneurysm hemodynamics: Impact of solver numerics versus mesh and time-step resolution,” *Am. J. Neuroradiology* **36**, 1310–1316 (2015).
- ²²P. Reymond, F. Merenda, F. Perren, D. Rüfenacht, and N. Stergiopoulos, “Validation of a one-dimensional model of the systemic arterial tree,” *Am. J. Physiol.: Heart Circ. Physiol.* **297**, H208–H222 (2009).
- ²³P. Reymond, Y. Bohraus, F. Perren, F. Lazeyras, and N. Stergiopoulos, “Validation of a patient-specific one-dimensional model of the systemic arterial tree,” *Am. J. Physiol.: Heart Circ. Physiol.* **301**, H1173–H1182 (2011).
- ²⁴*Vascular Ultrasound: How, Why and When*, 2nd ed., edited by A. Thrush and T. Hartshorne (Elsevier, 2005).
- ²⁵C. Huang, M. R. Lowerison, F. Lucien, P. Gong, D. Wang, P. Song, and S. Chen, “Noninvasive contrast-free 3D evaluation of tumor angiogenesis with ultrasensitive ultrasound microvessel imaging,” *Sci. Rep.* **9**, 4907 (2019).
- ²⁶J. Zhu, E. M. Rowland, S. Harput, K. Riemer, C. H. Leow, B. Clark, K. Cox, A. Lim, K. Christensen-Jeffries, G. Zhang, J. Brown, C. Dunsby, R. J. Eckersley, P. D. Weinberg, and M.-X. Tang, “3D super-resolution US imaging of rabbit lymph node vasculature in vivo by using microbubbles,” *Radiology* **291**, 642–650 (2019).